All-or-none disconnection of pyramidal inputs onto parvalbumin-positive interneurons gates ocular dominance plasticity

Authors: Daniel Severin[1†], Su Z. Hong[1†], Seung-Eon Roh[2†], Jiechao Zhou[2], Michelle C. D. Bridi[1], Ingie Hong[2], Sachiko Murase[3], Sarah Robertson[3], Rebecca Haberman[4], Richard Huganir[2], Michela Gallagher[4], Elizabeth M. Quinlan[3], Paul Worley[2], Alfredo Kirkwood[1,2].

[1]Mind/Brain Institute
Johns Hopkins University
Baltimore, MD 21218, USA

[2]Department of Neuroscience
Johns Hopkins University
Baltimore, MD 21205, USA

[3]Department of Biology
University of Maryland
College Park, MD 20742, USA

[4]Department of Psychological and Brain Sciences
Johns Hopkins University
Baltimore, MD 21218, USA

† Equally contributing authors

***Contact**: Correspondence should be addressed to Alfredo Kirkwood (Kirkwood@jhu.edu)

ABSTRACT

Disinhibition is an obligatory initial step in the remodeling of cortical circuits by sensory experience, yet the underlying mechanisms remain unclear. Our investigation of mechanisms for disinhibition in the classical model of ocular dominance plasticity (ODP) uncovered an unexpected novel form of experience-dependent circuit plasticity. In layer 2/3 of mouse visual cortex monocular deprivation triggers an "all-or-none" elimination of approximately half the connections from local pyramidal cells onto parvalbumin-positive interneurons (Pyr→PV), without affecting the strength of the remaining connections. This loss of Pyr→PV connections is transient, lasting one day only, has a critical period commensurate with the ODP critical period, and is contingent on a reduction of neuropentraxin2 (NPTX2), which normally stabilizes Pyr→PV connections. Bidirectional manipulations of NPTX2 functionality that prevent/promote the elimination Pyr→PV connections also promote/prevent ODP. We surmise, therefore, that this rapid and reversible loss of local Pyr→PV circuitry gates experience-dependent cortical plasticity.

INTRODUCTION

Experience during a postnatal critical period is essential to properly shape the functional connectivity of cortical circuits. A canonical model of cortical plasticity confined to a postnatal critical period is the shift in ocular dominance and visual acuity following monocular deprivation (MD). MD decreases the strength of cortical responses evoked by stimulation of the deprived eye and increases the response to the non-deprived eye [1]. Prior research established that MD-induced changes result from the reorganization of excitatory glutamatergic synapses onto excitatory cortical pyramidal neurons, which is in turn regulated by an inhibitory GABAergic network composed of parvalbumin-positive inhibitory interneurons (PVs). The consensus is that a permissive level of inhibition from PV circuits in cortical layer 2/3 is required for plasticity at downstream excitatory synapses, and that inhibition above or below the permissive range constrains the response to MD [2-4]. Accordingly, very early in postnatal development, the initial strengthening of the inhibitory output of PVs is proposed to trigger the onset of the critical period. Recent studies suggest that at later stages, following the full maturation of PV output, the “permissive” level of inhibition is achieved by reducing the recruitment of PVs [5-7].

The notion that disinhibition can initiate plasticity in mature cortical circuits originated from studies in primates showing that deafferentation and sensory deprivation can rapidly change GABAergic neuron output and morphology [8-10]. More recently, research in rodent visual cortex revealed that a reduction in the activity of PVs in layer 2/3 precedes and is necessary for the shift in ocular dominance induced by monocular deprivation [7]. Disinhibition of excitatory cortical neurons could be achieved indirectly, for example by suppressing PV-IN activity via enhancing inhibition from other interneurons through cholinergic neuromodulation [11, 12]; or more directly, by reducing the excitatory input onto PVs. Indeed, in the case of visual cortex,

manipulation of signaling pathways enriched at excitatory connections onto PV-INs revealed that weak excitatory drive is a permissive factor in the induction of ocular dominance plasticity [6, 13]. Our search for the mechanisms underlying disinhibition uncovered a novel form of experience-dependent plasticity that regulates the structural and functional connectivity between pyramidal neurons and PVs. We found that the initial response to monocular deprivation is a transient disconnection of ~50% of local pyramidal neurons to PV-INs in an “all-or-none” fashion, and that this complete structural and functional disconnection is an obligatory step for subsequent shifts in ocular dominance.

RESULTS

Brief MD transiently reduces local connectivity between Pyrs→PVs. We evaluated how monocular deprivation (MD) affects the connectivity between pyramidal neurons (Pyr) and PV interneurons (Pyrs→PVs) in mouse layer 2/3. To that end, we performed visualized whole cell-paired recordings in slices containing the monocular zone of V1 of mice expressing Td tomato in PVs (Fig. 1a,b. See methods). Consistent with previous studies [5, 14], in juvenile mice (p24-p30) the connection probability in proximate Pyr→PV pairs (less that 50 μm apart) was high (p~0.5) in slices from normal reared (NR) mice. In mice subjected to MD for 1 day (MD1) connection probability was reduced in the V1 contralateral to the deprived eye (Fig. 1c), but only for the pairs less that ~25 μm apart. A logistic regression analysis confirmed the significance of these differences (|Z|=3.228; p=0.0012), including the interaction between experience and Pyr-PV distance (|Z|=2.435; p=0.0149). In contrast, MD1 did not affect the connectivity in the non-deprived (ND) cortex ipsilateral to the deprived eye (NR-ND: p=0.6005). Using this ND cortex as a control we found the disconnection in deprived cortex is transient: the differences between cortices are significant after 1 day, but not after 2 and 3 days of MD (Logistic regression: (|Z|=2.370; p=0.0178; interaction between experience and days |Z|=2.020; p=0.0434; Fig. 1d). Importantly, the amplitude of the unitary excitatory postsynaptic current (uEPSC) of the proximal pairs that remained connected (within 12-24 microns) was not affected by MD (Fig. 1f). Moreover, MD did not affect crucial determinants of the uEPSC amplitude, including the quantal size, failure rate, and the size and replenishment rate of the readily releasable vesicle pool

(Supplementary Fig. 1). Finally, we found that in the binocular zone MD(1) also reduces the Pyr→PV connection probability, from 0/69±0/09 (N=5 mice, 29 pairs) in NR mice to 0.40±0.09 in MD mice (N=5,42; p=0.029. Data not shown).

Layer 2/3 PVs are also driven by excitatory inputs from layer 4 [15]. Since the probability of detecting connected intralaminar Pyr→PV pairs is typically very low (2 out of 20; not shown), we examined the effects of MD by computing the amplitude of maximal compound EPSCs as a measure of total strength in NR and MD mice [5, 16]. MD(1) reduced the amplitude of the maximal EPSC recruited electrically from layer 2/3 but not the EPSC recruited from layer 4 (Fig. 2c-g). Next, we evaluated changes in the ratio of EPSCs evoked in nearby Pyr and PVs by optogenetic stimulation of layer 4 inputs (Feldman). MD(1) did not affect the EPSC ratio in PV/Pyr (Fig. 2a,b). Since one day of MD does not affect excitatory inputs onto layer 2/3 pyramidal cells [7, 17], the absence of changes in the PV/Pyr ratio argues against alterations in layer 4 inputs to layer 2/3 PVs. Finally, we evaluated MD-induced changes in the outputs of PVs: PV→PV and PV→Pyr. MD(1) did not affect the amplitude of the maximal IPSC recorded in PVs (Supplementary Fig. 2a-c), the proportion of connected PV→Pyr pairs, nor the amplitude of the unitary IPSCs in Pyrs (Supplementary Fig. 2d-g). In sum, a primary effect of brief MD on Layer 2/3 PV circuitry is the selective and complete, yet transient, “all or none” elimination of approximately half the functional connections made by nearby pyramidal cells, without affecting the potency of the remaining connections.

Evidence that MD induces a transient structural loss of Pyr→PV connections. The “all or none” elimination of functional Pyr→PV connectivity is

reminiscent of synaptic pruning. Hence it suggests a loss of synaptic structure rather than a reduction in synaptic strength. To test this idea, we first considered the possibility that MD might "silence" Pyr→PV connections by inducing the removal of synaptic AMPA receptors, as has been documented in pyramidal neurons. To that end we compared the AMPA/NMDAR EPSC ratio, a crude indicator of changes in silent synapses, in PVs from deprived and non-deprived cortices. We detected no differences following MD1, arguing against a silent synapse scenario (Fig. 3a,b). Next, we evaluated changes in the number excitatory synapses onto PVs using immunocytochemistry to visualize the vesicular glutamate transporter 1 (VG1) as a marker for intracortical glutamatergic terminals. After 1 day of MD, the average number of VG1 puncta in the soma and proximal dendrites of PVs was reduced in deprived relative to non-deprived monocular zone, but there was no difference after 3 days of MD (Fig. 3b,c). These results suggest that MD causes a transient structural elimination of excitatory synapses onto PVs.

NPTX2 but not NRG1 mediates the disconnection of Pyrs→PVs by MD.

Attractive candidate mechanisms to mediate the disconnection of Pyr→PV synapses by MD include neuregulin1 (NRG1) and neuropentraxin2 (NPTX2) signaling. Both molecules are secreted by pyramidal neurons in an activity-dependent manner and promote/stabilize AMPARs at excitatory synapses onto PVs in multiple brain regions, including the visual cortex [5, 6, 18, 19]. A reduced secretion of NRG1 during MD has been associated with diminished excitatory input onto PV-INs [13]. We therefore tested whether supplemental NRG1 (1μg subcutaneous [6]) prevents the disconnection of Pyr→PV

during MD(1). Systemic NRG1 did not inhibit the decrease in Pyr→PV connection probability in deprived V1 after MD1 (Fig. 4a). Next, we examined how exogenous NRG1 affects excitatory inputs onto layer 2/3 PVs in slices from MD1 mice. To that end we recorded in the same PVs the EPSCs evoked by layer 2/3 and layer 4 stimulation. NRG1 application specifically enhanced the inputs from layer 4 (Fig. 4b), which are normally not affected by MD (see Fig. 2). A comparable enhancement of layer 4 inputs was also observed in normal reared V1b (Fig. 4 c). Together this argues against a role for NRG1 in the elimination of Pyr→PV connections in layer 2/3 by MD1.

Genetic ablation of NPTX2 (also known as NARP) has been shown to result in the all-or-none elimination of a substantial proportion of Pyr→PV connections (Gu et al, 2013). To examine the role of NPTX2 in the disconnection induced by MD, we monitored how MD changes the release NPTX2 *in vivo*. NPTX2 release was monitored by viral expression of NPTX2 fused with Super Ecliptic pHlurorin (SEP) which fluoresces only in the extracellular compartment [20]. In wild type mice virally transfected with AAV-CaMKII-NPTX2-SEP in V1, two-photon imaging in the superficial cortical layers revealed discrete puncta (2-3 μm) likely representing extracellular aggregates of NPTX2-SEP (Fig. 5b). One day of MD substantially reduced the density and intensity of these puncta, which returned to normal levels by the 2nd day of MD (Fig. 5b-d). A reduction in NPTX2 protein content in V1 after one day of MD is also revealed by quantitative immunochemistry (supplementary Fig. 4). These results suggest that MD transiently reduces the synaptic expression of NPTX2.

To test whether an MD-induced reduction in NPTX2 content is necessary for the Pyr→PV disconnection, we exploited the fact that the effects of MD on Pyr→PV-IN

inputs have a critical period. The loss of connectivity induced by one day of MD are robust up to postnatal day 50 (p50) but cannot be elicited at ~p100 (Fig. 6a). We therefore tested whether overexpression of NPTX2 prevents the MD-induced Pyr→PV disconnection in juveniles, and whether reducing the functionality of NPTX2 enables the disconnection in adults. In the first case we transfected V1 neonatally with AAV-CaMKII-NPTX2-SEP, in the second case we transfected V1 in adults with AAV2/2.CAMKII.dnNPTX2.EGFP to express a dominant negative form of NPTX2 that disrupts biosynthesis of the native NPTX1/2/R complex [21]. In juveniles (p21-p25) overexpressing NPTX2-SEP, the Pyr→PV connectivity remained high after MD(1), comparable to age-matched normal-reared controls (Fig. 6b). As a control we confirmed reduced connectivity after MD(1) in juveniles transfected with the same serotype AA virus expressing GFP (AAV2-CaMKII-GFP). On the other hand, in post-critical period adults (~p110) the expression of dnNPTX2, which by itself did not affect the Pyr→PV connectivity, enabled a substantial and significant disconnection of Pyr→PV inputs following MD(1) (Fig. 6c). As in the case of critical period mice the amplitude of the remaining EPSCs was normal (Fig. 6c). These results support a model in which a reduction of NPTX2 is a necessary permissive factor for the MD-induced disconnection of Pyr→PV inputs in layer 2/3.

Manipulation of NPTX2 prevent/enables ocular dominance plasticity. Finally, we examined whether the manipulations of NPTX2 that prevent/enable the Pyr→PV disconnections also prevent/enable the plasticity of ocular dominance (ODP) induced by MD. In mice, ODP induced by MD has a critical period with a time course parallel to the

time course for MD-induced disconnections of Pyr→PV inputs in layer 2/3 (Fig. 6a). ODP in the critical period is manifest as a rapid reduction of cortical responsiveness to the deprived eye in juveniles (younger than ~p35), and a delayed increase responsiveness to the non-deprived eye in young adults (younger than ~p70; [22, 23]. First, we asked how overexpression of NPTX2 following neo-natal AAV transfection (as in Fig. 6b), affects ocular dominance shift induced by brief MD in juveniles (3 days Fig. 7a). We used intrinsic signal imaging to evaluate cortical responses in the binocular zone of V1 as described [24, 25]. Cortical responses in mice are normally biased toward the contralateral eye and this bias is reduced by MD, reflected as a shift of the ocular dominance index (ODI, see methods). In NPTX2-transfected mice, the ODI for normal-reared and MD individuals was similar (Fig. 7b) and within the range for normal reared non transfected mice (Fig. 7b, light gray bar). On the other hand, mice transfected with control AAV and subjected to MD(3) exhibited a reduction in ODI, comparable to the decrease in ODI induced by MD3 in non-infected controls Fig. 7b, dark gray bar). In a complementary study we determined that transfecting adult mice (>p110) with AAV-dnNPTX2 to reduce NPTX2 function (as in Fig. 6c), enables a juvenile-like decrease in ODI in response to MD. In these experiments we imaged V1b before and after MD(3) (Fig. 8a) and confirmed that the reduction in ODI was juvenile-like; that is, it resulted from a reduction in the contralateral response, not from an increase in the ipsilateral response (Fig. 8b-e). Altogether, the results indicate that a loss of NPTX2-dependent Pyr→PV-IN connectivity is an obligatory early step in ODP.

DISCUSSION

Deprivation studies indicate that rapid disinhibition of pyramidal neurons enables plasticity of glutamatergic networks. Here we describe a novel form of synaptic plasticity that mediates cortical disinhibition induced by monocular deprivation: the “all-or-none” elimination of a subset of Pyr→PV connections. This “all-or-none” elimination of Pyr→PV inputs is distinct from most other models of synaptic weakening, in that all synaptic contacts between affected pairs of neurons are lost. Pyr→PV synapse elimination also contrasts with perinatal pruning of exuberant inputs [26-28] in that it is transient, lasting only one day, and it is not accompanied by a compensatory increase in the strength of the remaining inputs. In addition, the elimination of Pyr→PV inputs is also unique in that it is highly specific, affecting only inputs from nearby layer 2/3 pyramidal neurons, leaving inputs from distant pyramidal neurons in layer 2/3 or in layer 4 unchanged. Finally, the Pyr→PV input elimination is contingent on a reduced NPTX2 content, and it is a seemingly obligatory step for subsequent changes in ocular dominance.

The observation that the MD-induced change in Pyr→PV-IN inputs is both all-or-none, and transient, is somewhat counter intuitive, and it is unclear how temporary input elimination best serves ODP. Nevertheless, it seems plausible that the process is initiated by changes in neural activity resulting from diminished visual drive during MD. A reduced correlation of pre-postsynaptic activity in Pyr→PV pairs after MD is expected to induce associative long-term synaptic depression in these connections [29, 30] and may promote synapse elimination as reported in other types of depressed synapses [31, 32].

We propose that the reduction in the availability of NPTX2 induced by MD contributes to the destabilization of depressed Pyr→PV inputs in V1. Notably, associative LTD in Pyr→PV connections and synapse elimination in CA1 pyramidal cells require mGluR5 activation [30, 33], raising the possibility that the elimination of individual synapses and cell-to-cell connections share common initial mechanisms. The elimination of Pyr→PV inputs is highly local, occurring only in layer 2/3 Pyr→PV pairs separated by less than ~25□m. This spatial requirement matches the diameter of recently reported microcolumns in mouse cortex, suggesting that the distribution of disconnected synapses might reflect the co-regulation of locally connected neuronal networks [34]. The preferential local elimination might also be attributed to cortical retinotopy, as the decrease in correlated activity during MD might be more pronounced in proximal than distal pairs. The absence of an overt change in connectivity between layer 4 Pyrs→layer 2/3 PVs following MD may be due to low expression of NPTX2 in layer 4 neurons (Allen brain Mouse Atlas). Finally, the loss Pyr→PV inputs might be transient because subsequent homeostatic changes in glutamatergic synapses might restore patterns of neural activity conducive to re-establish connectivity [35-38].

Previous studies, including ours [6, 13] have implicated the growth factor NRG1 in plastic changes induced my MD. In contrast, here we show that application of exogenous NRG1 neither prevented nor restored the transient disconnection of MD-induced local Pyr→PV inputs in layer 2/3, arguing against a direct role of NRG1 in this process. A recent report utilizing a glutamate uncaging approach reported that applied NRG1 can restore a widespread reduction of excitatory input onto layer 2/3 PVs induced by MD(1) [13]. However, the uncaging approach can recruit and record

responses with a large polysynaptic component and the paired whole cell recordings used here may be preferable for resolving local monosynaptic connections. An attractive and simple possibility to reconcile these apparent discrepancies is that MD induces a NPTX-dependent disconnection of local Pyr-PV inputs in layer 2/3, and a NRG1-dependent reduction in local excitatory inputs onto layer 4 PVs. This would be in line with the notion that distinct mechanisms govern synaptic plasticity in different cortical layers [39-41], and is consistent with our observation that NRG1 affects excitatory inputs onto layer 2/3 PVs originating from layer 4, but not layer 2/3. If correct this scenario allows for two molecularly distinct mechanisms to regulate excitatory inputs onto PVs, that are anatomically segregated, thereby minimizing functional redundancy.

The rapid and transient elimination of approximately 50% of the local excitatory inputs onto Ps is likely a major determinant of the deprivation-induced cortical disinhibition attributed to the reduced activity of PVs [7, 42], However, other mechanisms might also contribute. For example, even if the strength and connectivity of the PV output is not affected by MD(1) (supplementary Fig. 2), changes in short-term synaptic dynamics, normally tuned for high frequency transmission [43], could enhance cortical activity. Similarly, changes in the electrical coupling between PVs, and tonic inhibition, known to be affected by deprivation in pyramidal neurons [44], could enhance cortical activity.

The critical periods for ocular dominance plasticity (Huang et al., 2015; Huang et al., 2010) and the plasticity of Pyr→PV-IN connectivity are highly coincidental, both terminating by p90. Furthermore, manipulations of NPTX2 function that prevent and promote the transient disconnection of Pyr→PV-IN inputs also prevent/promote ocular

dominance shift after MD. We therefore surmise that the transient elimination of local Pyr→PV inputs is an obligatory initial step for the subsequent remodeling of glutamatergic circuitry underlying ocular dominance plasticity.

An attractive candidate step to follow the loss of Pyr→PV connections could a rapid increase in the proportion of synaptic GluN2b over GluN2a subunit, which is observed after brief visual deprivation [35, 45]. The change in NMDAR composition lowers the threshold for the induction of synaptic plasticity, including LTP and LTD elicited with spike-timing protocols, and is consequence of cortical disinhibition [35, 45]. In this scenario, glutamatergic connectivity would not be intrinsically more plastic during the critical period, but plasticity is enabled by the change in GluN2b/GluN2a following the local elimination of Pyr→PV inputs. The termination of the critical period for ODP, would therefore be a direct consequence of the loss of plasticity of the Pyr→PV inputs. In this general context, it will be of interest to determine whether NPTX2-dependent disconnection of Pyr→PV inputs also regulates other candidate mechanisms of ODP, like the abundance of silent synapses [46]. Finally, it will be also of interest to examine whether disconnection of local Pyr→PV inputs contributes to the changes in cortical criticality after MD [42] and to pathology in neurological conditions known to exhibit marked alterations in NPTX2 abundance, including Alzheimer disease and schizophrenia [47].

FIGURE LEGENDS

Fig. 1 | MD transiently eliminates functional connections between local Pyr→PVs. **a,** Paired whole cell recordings from cortical slices containing deprived (D), non-deprived (ND) or normal-reared (NR) monocular V1. **b,** Example of uEPSCs (individuals: gray; average: black) evoked in a PV-IN (PV) by action potentials produced in pyramidal neuron (Pyr). **c**, probability that Pyr→PV pairs are synaptically connected versus distance between somas. Lines: 21 points running averages; symbols: binned averages over 10 μm (NR: white; D(1 day): black; ND: blue). **d**, Transient changes in functional connectivity during MD. The difference in pair connectivity between the D and ND hemispheres was significant following 1 day of MD only ($\chi^2[3\times2]=10.84$ p=0.0547; F-test MD(1) p=0.0139; F-test MD(2) p=0.7311; F-test MD(3) p>0.9999). **e**, uEPSC magnitude versus soma separation between Pyr and PV-IN. Spearman correlation (r_s) is not significant for either NR (white, p=0.1722) and D pairs (black, p=0.6710). **f**, MD does not affect the uEPSC magnitude of the connected pairs separated by > 12 μm and < 24 μm (light grey zone in c). NR: 28.0 ±3.5 pA; D(1): 24.6 ±3.1 pA; MW-test: U=222.5, p=0.7294). Traces are averaged uEPSCs (± 95% C.I) for all connected pairs. The number of pairs and mice is indicated in parenthesis in c,d,f.

Fig. 2 | MD(1) selectively reduces intralaminar excitatory inputs onto layer 2/3 PVs without affect ascending inputs from layer 4. a, Example EPSCs evoked in neighboring PVs and Pyrs by activating layer 4 inputs with optogenetic stimulation of increasing intensities (see methods for details). **b,** The response ratio (PV/PV+Pyr) was similar across stimulation intensities, and similar in pairs from NR (open circles) and D

(filled circles) mice (ANOVA F[1,128]=0.0007, p=0.9794; interaction F[5,128]=0.49, p=0.7844). Averages are shown as circles ±. s.e.m. **c-d**, Maximal EPSCs (EPSCmax) evoked by electrical stimulation of increasing intensity applied to layer 2/3 (black) or layer 4 (red), shown in **c**, were computed from input/output plots (shown in **d**). **e,** MD(1) reduced the EPSCmax evoked from layer 2/3 (NR:1.525±0.143nA, D: 0.986±0.156nA; MW-test U=97, p=0.0047). **f**, MD(1) did not reduce the EPSCmax evoked from layer 4 (NR: 1.380±0.122; D:1.356 ±0.113; t-test t=0.1464, p=0.8843. **g**, MD(1) reduces the ratio of EPSCmax evoked from layer 2/3/ layer 4. Circles in **e,f,g**: EPSCmax from individual cells; boxes: averages ± s.e.m. The number of cells or cell pairs and mice is indicated in parenthesis in **b,e,f,g.**

Fig. 3 | MD(1) induces a transient loss of structural Pyr→PV connections. a-b, Evidence against change in silent synapses. **a**, Schematic for measurement of NMDAR and AMPAR epscs. **b**, MD(1) does not affect the NMDAR/AMPAR (N/A) EPSC amplitude ratio (t-test F[29]=0.03165, p=0.9750). The number of cells and mice is indicated in parenthesis. **c-d,** Immunohistochemical analysis of the MD-induced changes in the VGlut1 puncta density on the soma and proximal dendrites of layer 2/3 PV-INs. **c**, Example cases (projection of 3 image planes) showing PV in red, VG1 in green. Colocalized puncta are depicted in yellow. **d**, Quantification of colocalized PV+VG1. The grey lines connect results of the deprived (D) and non-deprived (ND) monocular V1 of the same mouse after MD for 1 day (left) or 3 days (right). Averages are shown as circles connected by black lines ± s.e.m.

Fig. 4 | NRG1 does not affect inputs onto PVs from layer 2/3 Pyrs. a, In mice between p21-25 systemically injected with NRG1 (1μg/mouse subcutaneous, 1X prior to eye suture and 1X 1h before sacrifice; MD(1) reduces the Pyr→PV connection probability. Gray bars indicate the 95% CI in non-injected mice (data from Fig 1). **b**, In slices from MD mice, superfusion of NRG1 (5 nM grey zone) selectively potentiated EPSCs evoked from layer 4 (red symbols: 126.0±7.3% at 10-20 min. Wilcoxon test W=78, p=0.0005) without affecting EPSCs evoked from layer 3 (black symbols: 103.3±3.9%, Wilcoxon test W=16, p=0.5547). Left: average time course; right: grey lines connect EPSCs evoked by layer 4 and layer 3 stimulation in the same cell; the black lines connect averages ± s.e.m. **c,** NRG1 (5 nM grey zone) also potentiates EPSCs evoked by layer 4 stimulation in slices from normal-reared mice. Red symbols: electrically-evoked EPSCs; blue symbols: optogenetically-evoked EPSPs in mice expressing ChR2 in layer 4 (see methods). Left: average time course. Right: changes in individual cells; boxes: averages ± s.e.m; shaded red box: 95% C.I. for layer 4-evoked EPSCs in deprived slices (from 4b). Number of cells or cell pairs and mice is indicated in parenthesis in **a-c.**

Fig. 5 | MD transiently reduces surface Nptx2 in L2/3 V1. a, Time schedule of the experiment. AAV-CaMKII-NPTX2-SEP was injected into the visual cortex of wild-type mice at P30. Intrinsic signal imaging was carried out at P40 to identify V1. Around P47, live animals were imaged in layer 2/3 with 2-photon microscopy. **b,** Example images from the same mouse before and after 1, 2, and 3 days of MD reveals a brief reduction

of the number of NPTX2-SEP puncta at day 1. **c,** Quantification of NPTX2-SEP puncta number in L2/3 (80 -180μm) indicates a significant and transient reduction at day 1 (Repeated measures ANOVA F[1.508, 6.031]= 12.61, p=0.0087). **d,** The quantified total fluorescence intensity (in arbitrary units) of the NPTX2-SEP puncta is transiently reduced by 1 day MD (Repeated measures ANOVA F[1.132, 4.526]= 7.209, p=0.0466. Comparisons indicated in **c,d** used the Holm-Sidak's multiple comparison test. Grey lines in **c,d** represent data from individual mice; N = 5 mice; circles and black lines, average ± s.e.m.

Fig. 6 | Manipulations of NPTX2 prevent/enable MD-induced Pyr→PV disconnection. a, Critical period for the MD-induced plasticity of Pyr→PV inputs. In mice younger than ~p60 MD but not in ~p110 mice, MD for 1 day reduces the EPSC max amplitude (red circles. 2-way ANOVA F[1, 106]=18.66, p<0.0001; interaction p=0.006) and the probability of connection (black circles. Logistic regression F[1,23]=8.835, p=0.0036; interaction F[1,23]=3.918, p=0.0500). Data shown as averages ± s.e.m (Open circles: NR mice; filled circles: D mice). **b**, Transfection with AAV2-CaMKII-NPTX2-SEP at ~ birth prevents MD(1)-induced disconnection of Pyr→PV inputs in juveniles. Top: experimental schedule. Bottom: Pyr→PV connection probability in normal reared (NR), deprived (D) mice transfected with NPTX2-SEP, and deprived mice transfected with control virus (AA2-GFP). **c**, transfection of V1 with AAV2-dnNPTX2 in adult mice enables the MD(1)-induced disconnection of Pyr→PV inputs.

Top: experimental schedule. Bottom: the connection probability in normal reared (NR) and deprived (D) transfected mice. For comparison, boxes in **b,c** depict the 95% CI range non-transfected mice (light grey: normal-reared; dark grey: deprived). The number of cells or cell pairs and mice is indicated in parenthesis in **a-c.**

Fig. 7 | Overexpression of NPTX2 prevents ocular dominance plasticity in juveniles. a, Mice were transfected at birth (p0-2) with AAV2-CaMKII-NPTX2-SEP or AAV2-GPP. Following 3 days of monocular deprivation starting at p30-p31, intrinsic signal responses to stimulation in each eye were recorded in the V1 contralateral to the deprived eye (see methods). **b,** In the NPTX2 transfected mice (black circles), the ocular dominance index (ODI: see methods) after MD(3) was comparable to non-deprived transfected mice (white circles), and larger than in deprived mice transfected with control AAV2-GFP (black triangles). ANOVA $F[3,23]=12.56$, $p=0.0019$; NR_{NPTX2}-$D(3)_{NPTX2}$ $p>0.9999$; $D(3)_{NPTX2}$-$D(3)_{GFP}$ $p=0.0217$). For comparison, boxes in **b** depict the 95% CI range of ODI of 44 NR and 8 D non-transfected juvenile mice after MD(1) (light grey: normal-reared; dark grey: deprived).

Fig. 8 | Expression of dnNPTX2 enables juvenile-like ocular dominance plasticity in adults. a, Adult mice were transfected (p110-118) with AAV2-dnNPTX2. The intrinsic signal responses to stimulation in each eye were recorded in the V1 contralateral to the deprived eye before and after 3 days of monocular deprivation starting at p109-p129. **b,** Example experiment. Left: vasculature pattern of the imaged region used for alignment. Middle: magnitude map of the visual response from the eye contralateral [C] or

ipsilateral [I] to the imaged hemisphere. Gray scale (bottom): response magnitude as fractional change in reflection $x10^4$. Arrows: L, lateral, R, rostral. Right: histogram of ocular dominance index (ODI) is illustrated in the number of pixels (x-axis: ODI, y-axis: number of pixels). **c-e**, Summary of changes in response amplitude of the deprived contralateral eye (left) and the non-deprived ipsilateral eye (middle), and the change of ODI (right) before (b) and after (a) MD. Thin line: individual experiments; thick line and symbols: average ± s.e.m. For comparison, boxes in **e** depict the 95% CI range of ODI of 15 non-transfected, adult mice (light grey: normal-reared; dark grey: deprived).

Competing Financial Interests: The authors have no competing financial interests

Author Contributions: D.S and M.C.D.B. collected and analyzed slice electrophysiology data. S.H., S-Y.R., I.H. and RH collected, analyzed and interpreted the imaging data, J.Z made the NPTX2 virusrs, S.M, S.R., R.H., M.G and E.M.Q collected, analyzed and interpreted the immunohistology and immunochemistry data. D.S., P.W., E.M.Q. and A.K. wrote the manuscript.

Acknowledgements: We thank HK Lee for valuable advice. Supported by grants R35 NS097966 to PW, PO1 AG009973 to M.G., R01EY016431 to EMQ, R01EY12124 to A.K., R01EY025922 to EMQ and AK

REFERENCES

1. Frenkel, M.Y. & Bear, M.F. How monocular deprivation shifts ocular dominance in visual cortex of young mice. *Neuron* **44**, 917-923 (2004).
2. Feldman, D.E. Inhibition and plasticity [news]. *Nat Neurosci* **3**, 303-304 (2000).
3. Jiang, B., Huang, Z.J., Morales, B. & Kirkwood, A. Maturation of GABAergic transmission and the timing of plasticity in visual cortex. *Brain Res Brain Res Rev* (2005).
4. Hensch, T.K. & Quinlan, E.M. Critical periods in amblyopia. *Vis Neurosci* **35**, E014 (2018).
5. Gu, Y.*, et al.* Obligatory role for the immediate early gene NARP in critical period plasticity. *Neuron* **79**, 335-346 (2013).
6. Gu, Y.*, et al.* Neuregulin-Dependent Regulation of Fast-Spiking Interneuron Excitability Controls the Timing of the Critical Period. *J Neurosci* **36**, 10285-10295 (2016).
7. Kuhlman, S.J.*, et al.* A disinhibitory microcircuit initiates critical-period plasticity in the visual cortex. *Nature* **501**, 543-546 (2013).
8. Hendry, S.H.C. & Jones, E.G. Reduction in number of immunostained GABAergic neurones in deprived-eye dominance columns. *Nature* **320**, 750-753. (1986).
9. Hickmott, P.W. & Merzenich, M.M. Local circuit properties underlying cortical reorganization. *J Neurophysiol* **88**, 1288-1301 (2002).
10. Levy, L.M., Ziemann, U., Chen, R. & Cohen, L.G. Rapid modulation of GABA in sensorimotor cortex induced by acute deafferentation. *Ann Neurol* **52**, 755-761 (2002).
11. Froemke, R.C., Merzenich, M.M. & Schreiner, C.E. A synaptic memory trace for cortical receptive field plasticity. *Nature* **450**, 425-429 (2007).
12. Letzkus, J.J.*, et al.* A disinhibitory microcircuit for associative fear learning in the auditory cortex. *Nature* **480**, 331-335 (2011).
13. Sun, Y.*, et al.* Neuregulin-1/ErbB4 Signaling Regulates Visual Cortical Plasticity. *Neuron* **92**, 160-173 (2016).
14. Lu, J., Tucciarone, J., Lin, Y. & Huang, Z.J. Input-specific maturation of synaptic dynamics of parvalbumin interneurons in primary visual cortex. *Proc Natl Acad Sci U S A* **111**, 16895-16900 (2014).
15. Xu, X. & Callaway, E.M. Laminar specificity of functional input to distinct types of inhibitory cortical neurons. *J Neurosci* **29**, 70-85 (2009).
16. Morales, B., Choi, S.Y. & Kirkwood, A. Dark rearing alters the development of GABAergic transmission in visual cortex. *J Neurosci* **22**, 8084-8090 (2002).
17. Goel, A. & Lee, H.K. Persistence of experience-induced homeostatic synaptic plasticity through adulthood in superficial layers of mouse visual cortex. *J Neurosci* **27**, 6692-6700 (2007).
18. Tsui, C.C.*, et al.* Narp, a novel member of the pentraxin family, promotes neurite outgrowth and is dynamically regulated by neuronal activity. *J Neurosci* **16**, 2463-2478 (1996).
19. Fazzari, P.*, et al.* Control of cortical GABA circuitry development by Nrg1 and ErbB4 signalling. *Nature* **464**, 1376-1380 (2010).
20. Martineau, M.*, et al.* Semisynthetic fluorescent pH sensors for imaging exocytosis and endocytosis. *Nat Commun* **8**, 1412 (2017).
21. Charbonnier-Beaupel, F.*, et al.* Gene expression analyses identify Narp contribution in the development of L-DOPA-induced dyskinesia. *J Neurosci* **35**, 96-111 (2015).

22. Cooke, S.F. & Bear, M.F. How the mechanisms of long-term synaptic potentiation and depression serve experience-dependent plasticity in primary visual cortex. *Philos Trans R Soc Lond B Biol Sci* **369**, 20130284 (2014).
23. Lehmann, K. & Lowel, S. Age-dependent ocular dominance plasticity in adult mice. *PLoS One* **3**, e3120 (2008).
24. Kaneko, M., Stellwagen, D., Malenka, R.C. & Stryker, M.P. Tumor necrosis factor-alpha mediates one component of competitive, experience-dependent plasticity in developing visual cortex *Neuron* **58**, 673-680 (2008).
25. Hong, S.Z., Huang, S., Severin, D. & Kirkwood, A. Pull-push neuromodulation of cortical plasticity enables rapid bi-directional shifts in ocular dominance. *Elife* **9** (2020).
26. Chen, C. & Regehr, W.G. Developmental remodeling of the retinogeniculate synapse. *Neuron* **28**, 955-966 (2000).
27. Patel, A.B., Loerwald, K.W., Huber, K.M. & Gibson, J.R. Postsynaptic FMRP promotes the pruning of cell-to-cell connections among pyramidal neurons in the L5A neocortical network. *J Neurosci* **34**, 3413-3418 (2014).
28. Kano, M. & Watanabe, T. Developmental synapse remodeling in the cerebellum and visual thalamus. *F1000Res* **8** (2019).
29. Lamsa, K.P., Kullmann, D.M. & Woodin, M.A. Spike-timing dependent plasticity in inhibitory circuits. *Front Synaptic Neurosci* **2**, 8 (2010).
30. Huang, S., Huganir, R.L. & Kirkwood, A. Adrenergic gating of Hebbian spike-timing-dependent plasticity in cortical interneurons. *J Neurosci* **33**, 13171-13178 (2013).
31. Henson, M.A., Tucker, C.J., Zhao, M. & Dudek, S.M. Long-term depression-associated signaling is required for an in vitro model of NMDA receptor-dependent synapse pruning. *Neurobiol Learn Mem* **138**, 39-53 (2017).
32. Oh, W.C., Hill, T.C. & Zito, K. Synapse-specific and size-dependent mechanisms of spine structural plasticity accompanying synaptic weakening. *Proc Natl Acad Sci U S A* **110**, E305-312 (2013).
33. Wilkerson, J.R.*, et al.* A role for dendritic mGluR5-mediated local translation of Arc/Arg3.1 in MEF2-dependent synapse elimination. *Cell Rep* **7**, 1589-1600 (2014).
34. Maruoka, H.*, et al.* Lattice system of functionally distinct cell types in the neocortex. *Science* **358**, 610-615 (2017).
35. Bridi, M.C.D.*, et al.* Two distinct mechanisms for experience-dependent homeostasis. *Nat Neurosci* **21**, 843-850 (2018).
36. Hengen, K.B., Lambo, M.E., Van Hooser, S.D., Katz, D.B. & Turrigiano, G.G. Firing rate homeostasis in visual cortex of freely behaving rodents. *Neuron* **80**, 335-342 (2013).
37. Lee, H.K. & Kirkwood, A. Mechanisms of Homeostatic Synaptic Plasticity in vivo. *Front Cell Neurosci* **13**, 520 (2019).
38. Keck, T., Hubener, M. & Bonhoeffer, T. Interactions between synaptic homeostatic mechanisms: an attempt to reconcile BCM theory, synaptic scaling, and changing excitation/inhibition balance. *Curr Opin Neurobiol* **43**, 87-93 (2017).
39. Fong, M.F.*, et al.* Distinct Laminar Requirements for NMDA Receptors in Experience-Dependent Visual Cortical Plasticity. *Cereb Cortex* **30**, 2555-2572 (2020).
40. Jiang, B., Trevino, M. & Kirkwood, A. Sequential development of long-term potentiation and depression in different layers of the mouse visual cortex. *J Neurosci* **27**, 9648-9652 (2007).
41. Frantz, M.G.*, et al.* Layer 4 Gates Plasticity in Visual Cortex Independent of a Canonical Microcircuit. *Curr Biol* **30**, 2962-2973 e2965 (2020).

42. Ma, Z., Turrigiano, G.G., Wessel, R. & Hengen, K.B. Cortical Circuit Dynamics Are Homeostatically Tuned to Criticality In Vivo. *Neuron* **104**, 655-664 e654 (2019).
43. Bridi, M.S., Shin, S., Huang, S. & Kirkwood, A. Dynamic Recovery from Depression Enables Rate Encoding in Inhibitory Synapses. *iScience* **23**, 100940 (2020).
44. Huang, S., Hokenson, K., Bandyopadhyay, S., Russek, S.J. & Kirkwood, A. Brief Dark Exposure Reduces Tonic Inhibition in Visual Cortex. *J Neurosci* **35**, 15916-15920 (2015).
45. Guo, Y.*, et al.* Dark exposure extends the integration window for spike-timing-dependent plasticity. *J Neurosci* **32**, 15027-15035 (2012).
46. Xu, W., Lowel, S. & Schluter, O.M. Silent Synapse-Based Mechanisms of Critical Period Plasticity. *Front Cell Neurosci* **14**, 213 (2020).
47. Xiao, M.F.*, et al.* NPTX2 and cognitive dysfunction in Alzheimer's Disease. *Elife* **6** (2017).

Figure 1

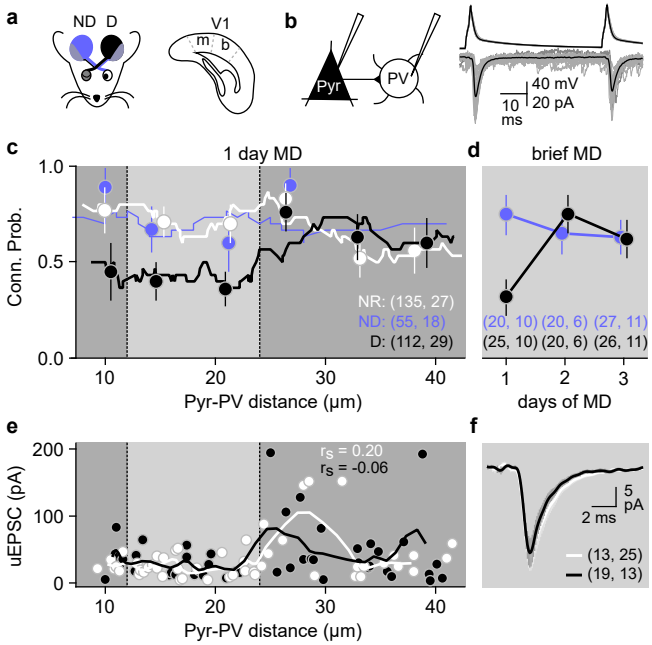
a
ND D
V1
m
b
b
Pyr
PV
40 mV
20 pA
10
ms
c
1 day MD
Conn. Prob.
1.0
0.5
0.0
NR: (135, 27)
ND: (55, 18)
D: (112, 29)
10
20
30
40
Pyr-PV distance (μm)
d
brief MD
(20, 10) (20, 6) (27, 11)
(25, 10) (20, 6) (26, 11)
1
2
3
days of MD
e
uEPSC (pA)
200
100
0
rs = 0.20
rs = -0.06
10
20
30
40
Pyr-PV distance (μm)
f
5
pA
2 ms
(13, 25)
(19, 13)

Figure 2

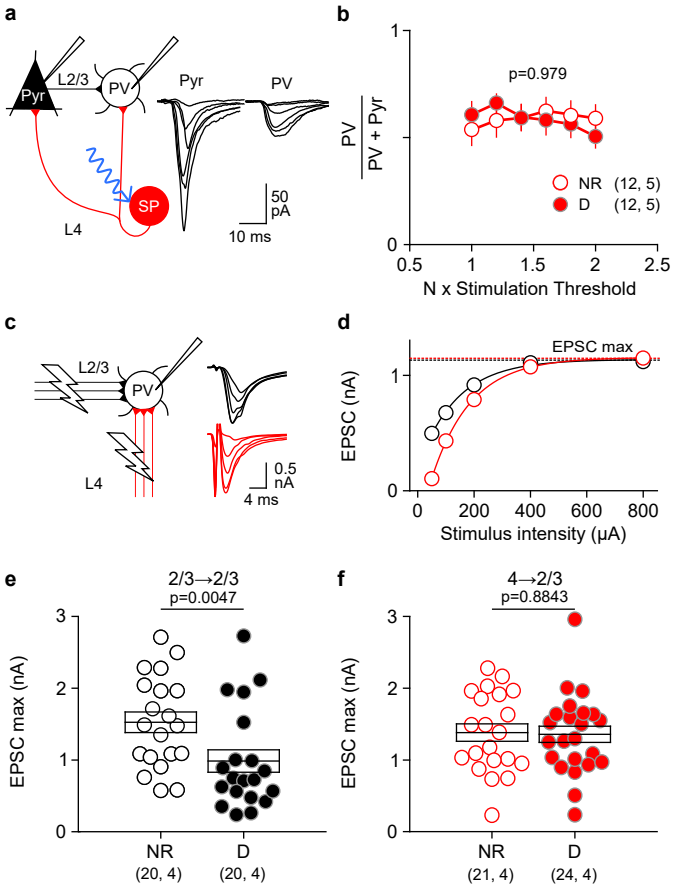
a
Pyr
L2/3
PV
Pyr
PV
SP
L4
50 pA
10 ms
b
p=0.979
PV / PV + Pyr
NR (12, 5)
D (12, 5)
N x Stimulation Threshold
c
L2/3
PV
L4
0.5 nA
4 ms
d
EPSC max
EPSC (nA)
Stimulus intensity (μA)
e
2/3→2/3
p=0.0047
EPSC max (nA)
NR (20, 4)
D (20, 4)
f
4→2/3
p=0.8843
EPSC max (nA)
NR (21, 4)
D (24, 4)

Figure 3

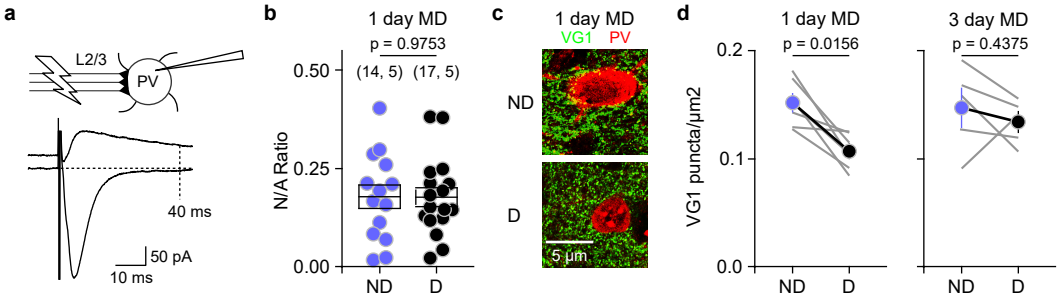
a
L2/3
PV
40 ms
50 pA
10 ms
b
1 day MD
p = 0.9753
(14, 5) (17, 5)
N/A Ratio
0.50
0.25
0.00
ND
D
c
1 day MD
VG1 PV
ND
D
5 µm
d
1 day MD
p = 0.0156
3 day MD
p = 0.4375
VG1 puncta/µm2
0.2
0.1
0.0
ND
D

Figure 4

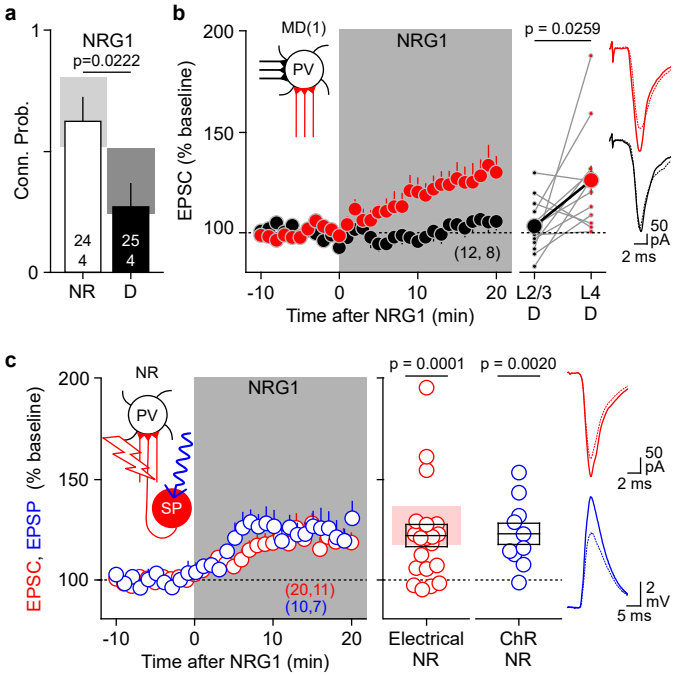
a
NRG1
p=0.0222
Conn. Prob.
1
0
24
4
25
4
NR
D
b
MD(1)
PV
NRG1
EPSC (% baseline)
200
150
100
(12, 8)
-10
0
10
20
Time after NRG1 (min)
p = 0.0259
L2/3
D
L4
D
50
pA
2 ms
c
NR
PV
SP
NRG1
EPSC, EPSP (% baseline)
200
150
100
(20,11)
(10,7)
-10
0
10
20
Time after NRG1 (min)
p = 0.0001
p = 0.0020
Electrical
NR
ChR
NR
50
pA
2 ms
2
mV
5 ms

Figure 5

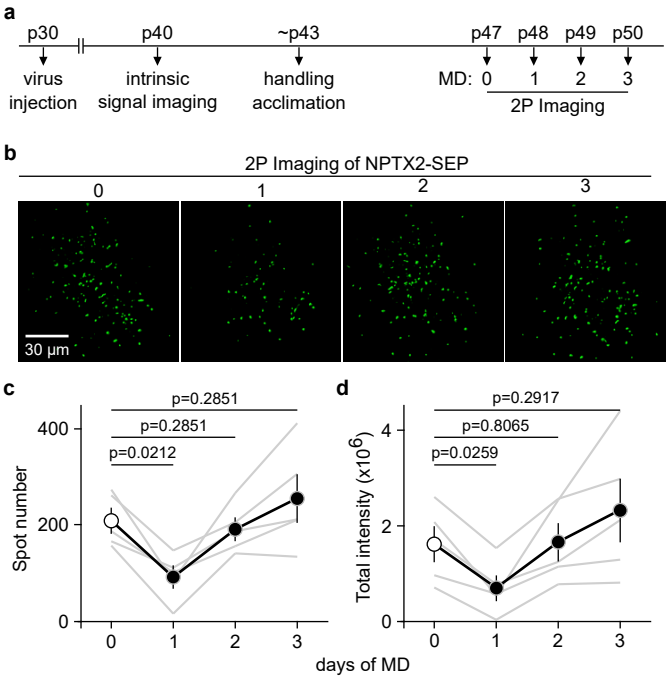
a
p30
p40
~p43
p47
p48
p49
p50
virus injection
intrinsic signal imaging
handling acclimation
MD: 0 1 2 3
2P Imaging
b
2P Imaging of NPTX2-SEP
0
1
2
3
30 µm
c
p=0.2851
p=0.2851
p=0.0212
Spot number
400
200
0
0
1
2
3
d
p=0.2917
p=0.8065
p=0.0259
Total intensity (x10^6)
4
2
0
0
1
2
3
days of MD

Figure 6

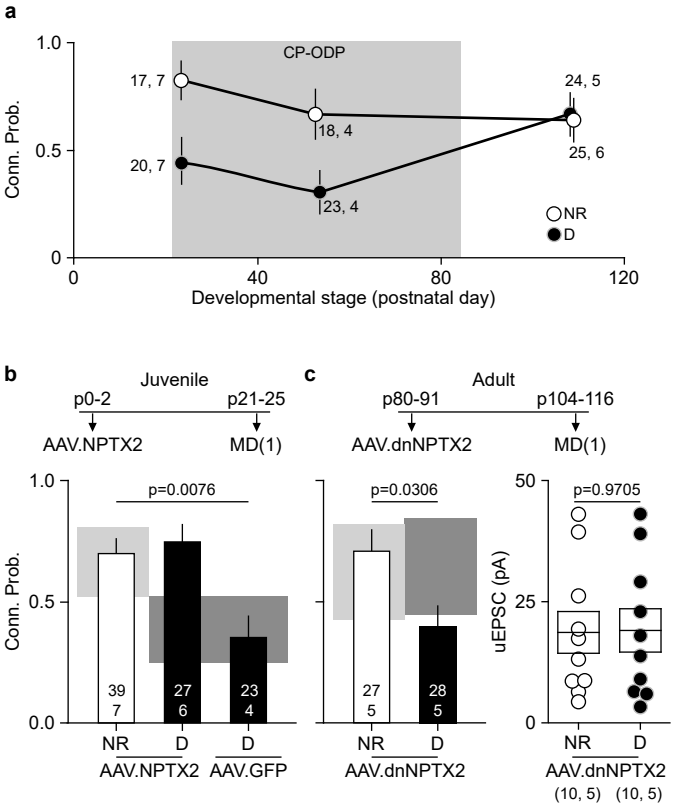
a
CP-ODP
Conn. Prob.
1.0
0.5
0
17, 7
18, 4
24, 5
25, 6
20, 7
23, 4
NR
D
0
40
80
120
Developmental stage (postnatal day)
b
Juvenile
p0-2
p21-25
AAV.NPTX2
MD(1)
p=0.0076
39
7
27
6
23
4
NR
D
D
AAV.NPTX2
AAV.GFP
c
Adult
p80-91
p104-116
AAV.dnNPTX2
MD(1)
p=0.0306
27
5
28
5
NR
D
AAV.dnNPTX2
uEPSC (pA)
50
25
p=0.9705
NR
D
AAV.dnNPTX2
(10, 5)
(10, 5)

Figure 7

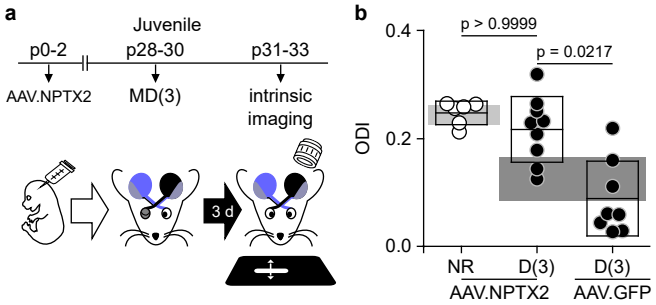
a
Juvenile
p0-2
p28-30
p31-33
AAV.NPTX2
MD(3)
intrinsic
imaging
3 d
b
p > 0.9999
p = 0.0217
ODI
0.4
0.2
0.0
NR
D(3)
D(3)
AAV.NPTX2
AAV.GFP

Figure 8

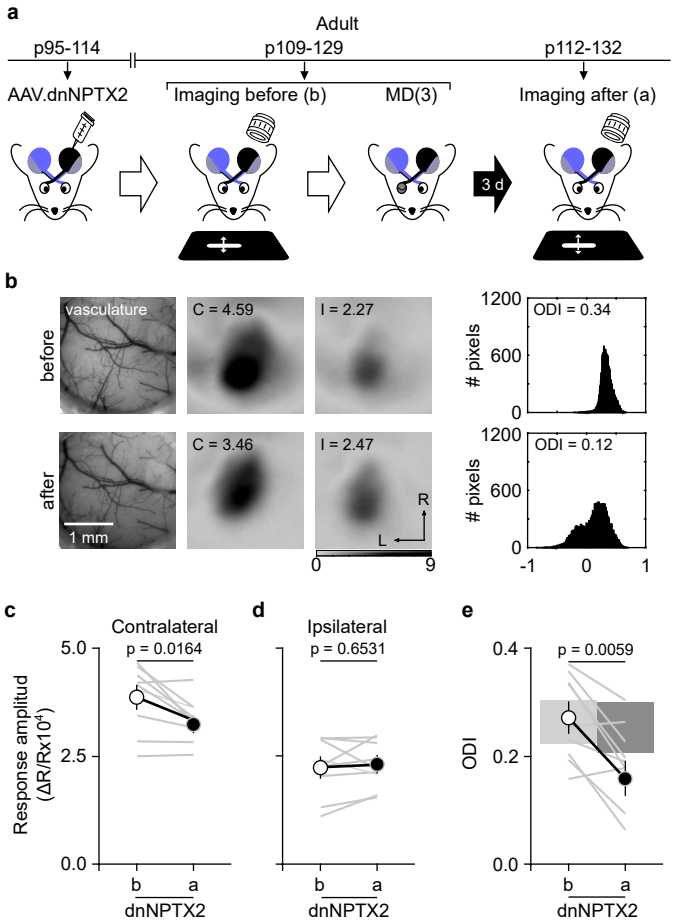
a
Adult
p95-114
p109-129
p112-132
AAV.dnNPTX2
Imaging before (b)
MD(3)
Imaging after (a)
3 d
b
before
after
vasculature
C = 4.59
I = 2.27
C = 3.46
I = 2.47
1 mm
R
L
0
9
ODI = 0.34
ODI = 0.12
# pixels
1200
600
0
-1
0
1
c
Contralateral
p = 0.0164
Response amplitud
(ΔR/Rx10⁴)
5.0
2.5
0.0
b
a
dnNPTX2
d
Ipsilateral
p = 0.6531
e
p = 0.0059
ODI
0.4
0.2
0.0